The reinforcement effects of PVA, PE, and steel fibers on AAS material

Xu, Yaowen; Wan, Chaojun; Liang, Xuhui; Yang, Hongyu

DOI
10.1016/j.cscm.2022.e01386

Publication date
2022

Document Version
Final published version

Published in
Case Studies in Construction Materials

Case Studies in Construction Materials 17 (2022) e01386

Contents lists available at ScienceDirect

Case Studies in Construction Materials

journal homepage: www.elsevier.com/locate/cscm

The reinforcement effects of PVA, PE, and steel fibers on AAS material

Yaowen Xu [a], Chaojun Wan [a,*], Xuhui Liang [b,*], Hongyu Yang [a]

[a] College of Materials Science and Engineering, Chongqing University, Chongqing 400045, PR China
[b] Department of Materials, Mechanics, Management & Design, Faculty of Civil Engineering and Geoscience, Delft University of Technology, Delft, the Netherlands

ARTICLE INFO

Keywords:
Fiber-reinforced AAS
Hybrid fiber
Strain-hardening
Crack
Uniaxial tension

ABSTRACT

This paper employs PVA, PE, steel fibers, as well as the hybrids of two of the three fibers to reinforce alkali-activated slag (AAS) material, aiming to prepare strain-hardening and clinker-free composites. The flexural strength, compressive strength, uniaxial tensile performance of the composites and bond behavior between fibers and the matrix were tested to clarify the reinforcement effects of different fibers on the matrix. Strain-hardening AAS materials are obtained with compressive strengths of 116 MPa − 137 MPa (with fibers contributions of 17%−38%) and strain capacities over 0.8% at 60 d. The results indicate that there are several kinds of reinforcement effects of fibers on the matrix, namely bridging effect, lapping effect (for steel fibers), synergetic effect (for hybrid fibers) and static effect (for flexible fibers). Deterioration of PVA and PE fibers are found, indicating that these two fibers have poor adaptability in AAS material with a high alkalinity. This paper specially distinguishes the difference of the crack numbers during the strain-hardening stage only with the ones during the whole period including the following strain-softening stage. A new relationship is established between the crack numbers and the strain-stress curves, which provides a more reasonable way to characterize the strain-hardening property of fiber-reinforced composites.

1. Introduction

Brittleness is one of the problems for cement concrete. Conventional concrete is prone to crack and consequently cause negative impacts on its durability. More seriously, the brittleness of conventional concrete is a potential threat to the safety of life and property as fractures and collapses may occur when concrete structures suffering catastrophes such as earthquakes, tsunamis, and explosions. There are two main ways to toughen concrete, minimizing defects (i.e. reducing the maximum pore and homogenizing internal structure) [1,2] and strengthening with fibers [3–6]. Engineered Cementitious Composite (ECC) is prominent in fiber-reinforced concrete due to its outstanding ductility, toughness, and strain-hardening behavior [6]. Differing from conventional concrete, ECC

Abbreviations: ECC, Engineered cementitious composite; OPC, ordinary Portland cement; AAMs, alkali-activated materials; AAS, alkali-activated slag; GGBFS, ground granulated blast furnace slag; FPVA, samples prepared with PVA fiber; FPE, samples prepared with PE fiber; FS, samples prepared with steel fiber; FAS, samples prepared with PVA and steel fiber; FAE, samples prepared with PVA and PE fiber; FSE, samples prepared with steel and PE fiber; σ_{tfc}, first cracking tensile strength; σ_{tu}, ultimate tensile strength; ε_{tu}, ultimate tensile strain; ε_{tfc}, first cracking tensile strain.

* Corresponding authors.
E-mail addresses: cjwan@cqu.edu.cn (C. Wan), X.Liang-1@tudelft.nl (X. Liang).

https://doi.org/10.1016/j.cscm.2022.e01386
Received 18 May 2022; Received in revised form 26 June 2022; Accepted 9 August 2022
Available online 10 August 2022

does not rupture immediately under the tensile load. Contrarily, the tensile stress of ECC increases with the increase of strain and usually, an ultimate tensile strength comes with a high ultimate tensile strain. ECC has a stable failure mode rather than a catastrophic failure mode, attributed to multiple cracking [7]. It's worth noting that although ECC is easy to crack, most of the crack widths are less than 60 μm, which are harmless to the durability of concrete and can be healed with further hydration of cement [8]. ECC is designed on the bases of micromechanics, fracture mechanics and statistics [7]. Tensile strength of 5–8 MPa, tensile strain of 3–5% can be achieved and strain capacity of 12% has been obtained in the laboratory [9–16]. The pore structure and the interfacial transition zone between fiber and matrix of ECC can be improved by adding admixtures such as silica fume, nano-SiO_2, or/and nano-$CaCO_3$ [17,18]. The investigations of ECC on self-consolidating [19], extruding [20], shotcreting [21,22], 3D printing [23], as well as hydrophobic property [24], fire-resistant [25,26], self-cleaning [27] have expanded its application in engineering.

ECC is attractive for good mechanical performance and durability, however, its high cement consumption caused by the absence of coarse aggregates makes it expensive and environmentally unfriendly. The cement content of a typical ECC mixture is about 600 kg/m^3 [28], which is much higher than that of the conventional concrete. High cement consumption (i.e. high clinker consumption) corresponds to high greenhouse gas emission. Therefore, it is necessary to try to reduce the cement content to develop green and sustainable ECC [29]. Supplementary materials such as slag and fly ash have been proved effective for partial substitution of cement and reduction of the environmental impact of ECC [30,31]. Besides, alternative binders could be more promising to replace ordinary Portland cement (OPC) to prepare green ECC. Among the candidates, alkali-activated materials (AAMs) are in the spotlight and have shown a large potential [32,33]. Several researches have been done to prepare clinker-free ECC by using AAMs, with tensile strains of 1.10%− 7.50% achieved [34–36], which are comparable with the cement-based ECC. However, the compressive strength is limited within 63.7 MPa [36] even though heat curing (60 °C for 24 h) is adopted, which undoubtedly, cannot meet the demand of high strength of building materials.

Alkali-activated slag (AAS) material, a kind of potential building material, is prepared with ground granulated blast furnace slag (GGBFS) and activators. Waterglass-activated slag can easily obtain high strength by design. Nevertheless, the different reaction products and microstructure between AAS and cement make the fiber-reinforced behavior in AAS different from that in the traditional ECC. Thus, the behavior of different fibers in the AAS matrix needs to be further studied.

To investigate the reinforcement effect of fibers on AAS material and obtain ductile strain-hardening green ECC with high strength, this study attempted to use three kinds of commonly used fibers for strain-hardening composites (i.e. PVA, PE and steel fibers) to reinforce AAS. The hybrids of two of these three fibers were also employed. The compressive strength, flexural strength, uniaxial tensile performance of the composites and bond behavior between fibers and the matrix were tested and investigated in this study.

2. Materials and methods

2.1. Materials

Blast furnace slag (supplied by Chongqing iron & steel (group) co. LTD) and fly ash (supplied by Chongqing huaneng luohuang power plant) were used as precursors. Blast furnace slag was ground in the vibration mill for about 40 min to get ground granulated blast furnace slag (GGBFS) before further study. The bulk densities of GGBFS and fly ash are 2.9×10^3 kg/m^3 and 2.2×10^3 kg/m^3, respectively. Table 1 lists the chemical compositions of GGBFS and fly ash. Waterglass was employed as activator, and its modulus was tailored by NaOH (AR) to 1.2. The super-fine sand (collected from the Yangzi River in Chongqing) had been washed and sieved before use. The fineness modulus of the super-fine sand is 1.07. Three kinds of fibers were employed to prepare fiber-reinforced AAS composites, namely PVA, PE, and steel fibers. The appearances and properties of the fibers are shown in Fig. 1 and Table 2, respectively.

2.2. Mix design

Table 3 shows the mix proportions. The mixture of matrix binder was determined based on our previous research, with multiple properties (i.e. the powder packing density, the fluidity of the paste, as well as the strengths of paste and mortar) comprehensively considered [37]. Group F0 is set as the reference group. Samples with one type of fiber are named by the corresponding fiber as FPVA, FPE, and FS. Samples with hybrid fibers are named FAS (PVA+Steel), FAE (PVA+PE), and FSE (Steel+PE). Mixing and casting procedures are as followed. GGBFS, fly ash and sand were firstly added into a planetary mixer and dry mixed for about 30 s. Then the activator was added and mixed for about 60 s. Finally, fibers were slowly added and continuously mixed for another 5 min. Once the mix was finished, the composite was cast into prism molds (40 ×40 ×160 mm) and dog bone shape molds (Fig. 2) and was then moderately vibrated to compact.

Samples were covered with plastic films to avoid moisture evaporation, and placed in the laboratory for about 24 h. Afterwards, samples were demolded and cured in a fog room with the temperature at 20 ± 2 °C and relative humidity exceeds 95% until to be tested.

Table 1
Chemical compositions of GGBFS and fly ash determined by chemical analysis according to GB/T 176–2008 [%].

	CaO	SiO_2	Al_2O_3	MgO	TiO_2	MnO	Fe_2O_3	K_2O	SO_3	LOI
GGBFS	37.09	32.69	14.14	7.79	3.35	1.25	1.05	0.49	0.48	1.67
Fly ash	3.40	40.02	25.30	0.49	–	–	15.40	–	0.77	4.62

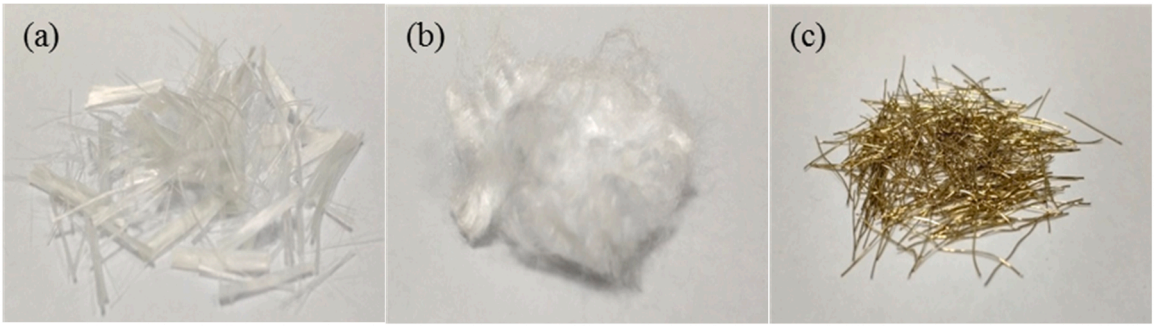

Fig. 1. The appearances of different fibers: (a) PVA fibers; (b) PE fibers; (c) Steel fibers.

Table 2
Properties of PVA, PE and steel fibers.

Fibers	Tensile strength (MPa)	Diameter (μm)	Length (mm)	Elastic Modulus (GPa)	Elongation (%)	Density (kg/m^3)
PVA	1620	39	12	42.8	6.0	1300
PE	3000	20	12	85	4.92	970
Steel	2500	200	12	200	–	7800

Table 3
Mix proportions of fiber-reinforced AAS composites.

Group	GGBFS	Fly ash	S/B[a]	W/B[b]	Modulus of water glass	A/B[c] (%)	Fibers (vol%)		
							PVA	PE	Steel
F0							0	0	0
FPVA							2	0	0
FPE							0	2	0
FS	0.95	0.05	0.7	0.35	1.2	8	0	0	2
FAS							1	0	1
FAE							1	1	0
FSE							0	1	1

[a] Sand to Binder ratio;
[b] Water to Binder ratio;
[c] Alkali to Binder ratio.

2.3. Experimental methods

2.3.1. Flexural and compressive strength

Flexural and compressive strengths of samples were tested according to GB/T 17671–1999, with loading rates of 50 N/s and 2.4 kN/s, respectively. Given that samples with fibers kept good shape after the compressive strength test, each sample was applied to a secondary compression loading. For groups FPE, FAS, FAE, and FSE, after suffering two times of compression loadings at the age of 3 d, samples were cured and then subjected to a third-time compression loading at the age of 60 d.

2.3.2. Uniaxial tensile test

The uniaxial tensile test setup is shown in Fig. 3. A dynamic strain gauge extensometer (Instron 2620–601) is used to gauge strain. The output sensitivity of the extensometer is 2.5 ± 20% mV/V. The electrical calibration accuracy is ± 0.10% full rated output. The loading rate was maintained at 0.2 mm/min until the sample failed. And the loading forces and elongations were measured and recorded.

2.3.3. SEM analysis

The bond behaviors between fibers and the AAS matrix were investigated by using VEGA3 TESCAN LMH SEM with the HV of 20.0 kV. The surface morphologies of original fibers were observed by using Quattro S Thermo Scientific SEM with the HV of 20.0 kV.

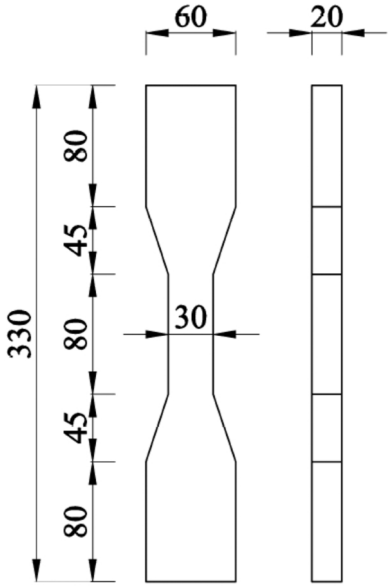

Fig. 2. The sample geometry for uniaxial tensile test (unit: mm).

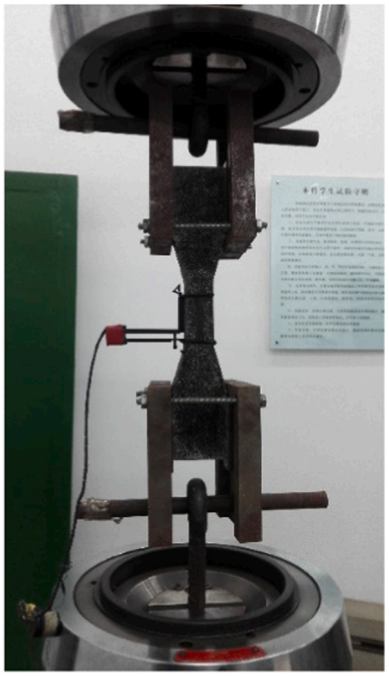

Fig. 3. The setup of uniaxial tensile test.

3. Results

3.1. Flexural strength

Fig. 4 shows the flexural strength of AAS material incorporated with different fibers at the age of 3 d and 60 d. Compared with group F0 without fibers, the increased ratios on flexural strength of group FPVA, FPE, FS, FAS, FAE and FSE at the age of 3 d are 86.9%, 34.5%, 10.7%, 75.0%, 65.5% and 86.9%, respectively, and at the age of 60 d are 225.0%, 263.5%, 121.2%, 246.2%, 257.7% and 255.8%, respectively. It should be noted that there is a strength decrease for group F0, i.e. the flexural strengths at the age of 60 d are lower than those at 3 d. The increased ratio on flexural strength for group FS is relatively lower. This is because compared with flexible

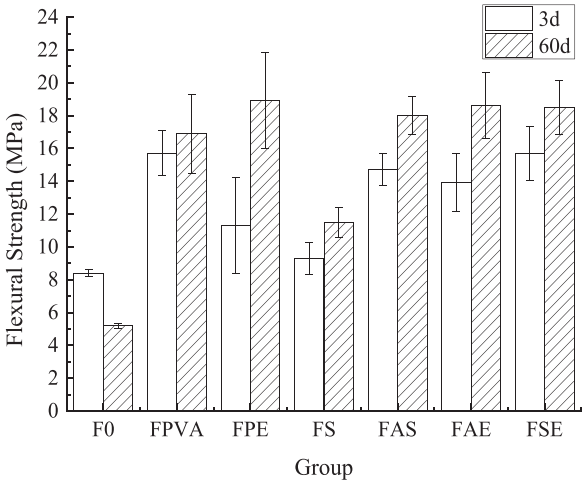

Fig. 4. The flexural strength of AAS material incorporated with different fibers at the age of 3 d and 60 d.

fibers (i.e. PVA and PE fibers), steel fibers are less capable to occur the coordination deformation with the matrix when samples are subjected to flexural loading, thus steel fibers are easy to be separated from the matrix. All of the fiber-reinforced AAS composites have the followed characteristics during flexural loading: (1) The load decreases slightly and then increases repeatedly, until reaching the peak value, followed by a slowly decrease which usually lasts a long duration; (2) After bending, the loading bottom surface of the sample presents one main crack with multiple micro-cracks as shown in Fig. 5, and the loading side surfaces of the sample have multiple radial micro-cracks.

3.2. Compressive strength

Fig. 6 shows the compressive strengths of AAS materials with and without fibers at the age of 3 d and 60 d. Compared with the group F0, the compressive strength of group FPVA at the age of 3 d (Fig. 6(a)) increases from 56.3 MPa to 74.6 MPa, with an increased ratio of 32.5%. The increased ratios of group FPE, FS, FAS, FAE and FSE are 36.8%, 38.5%, 49.6%, 34.1% and 48.1%, respectively. For the samples at the age of 60 d, as shown in Fig. 6(b), all the fiber-reinforced groups have compressive strength over 110 MPa. Compared with group F0, the increased ratios of compressive strength at the age of 60 d for the group of FPVA, FPE, FS, FAS, FAE and FSE are 17.5%, 18.1%, 38.4%, 20.2%, 17.4% and 25.6%, respectively.

The reason for the strength improvement of the flexible fibers to the matrix is bridging. Because of bridging, the disorderly distributed fibers can restrict the deformation of the matrix and mitigate the development of cracks, as well as change the transfer direction of stress. Besides, another reason for the strength improvement of steel fibers to the matrix is lapping. When the volume fraction of steel fibers exceeds a certain level, the lapping of fibers occurs. Lapping can also increase the loading capacity of samples.

The tensile strength of PE fibers (3000 MPa) is higher than that of PVA fibers (1620 MPa) (as shown in Table 2), hence the increased ratio of compressive strength of group FPE is higher than that of the group FPVA. When these two kinds of flexible fibers are mixed at the ratio of 1:1, the increased ratio is in between. The hybrid of flexible fibers and steel fibers increases the compressive strength compared with the group of FPVA, FPE or FS at 3 d, which means that there is a synergistic effect. However, this synergistic effect disappears at 60 d. This will be discussed in 4.1.

The hydrophobicity of the surface of fibers can also influence the effect of fibers on AAS material. For the hydrophilic PVA and steel fibers, dispersion in the matrix is easier. At the same time, water can be adsorbed on the fiber surface. The actual water to powder ratio

Fig. 5. The sample appearance after three-point bending test (the surface which contacts with two supporting points during bending).

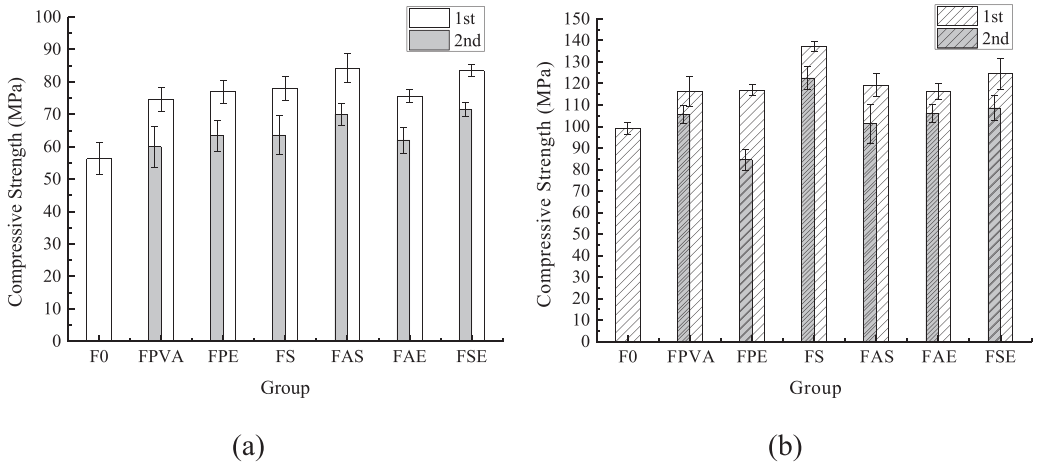

Fig. 6. The compressive strength of the first-time and second-time loadings of AAS material incorporated with different fibers at the age of: (a) 3 d; (b) 60 d. White bars represent the first-time loadings and grey bars represent the second-time loadings.

deceases consequently, which would result in higher compressive strength. By contrast, for the hydrophobic PE fibers with lightweight and cotton-like properties, dispersion is difficult. Thus the positive effect of PE fibers on the compressive strength of samples would be limited to some extent. Besides, adding PE fibers reduced the fluidity apparently but the value was not tested in this study.

The incorporation of fibers into AAS material not only improves the compressive strength but also changes their failure mode. The samples with fibers do not change apparently before and after loading. It is significantly different from group F0, which experiences explosion and collapse after the strength test. Because all the fiber-reinforced samples still retained shapes after suffering the first-time compressive loading, a second loading was conducted on each sample and the results are shown as the shadow column in Fig. 6. At the age of 3 d, the fiber-reinforced AAS composites at the age of 3 d can retain more than 80% of the compressive strength after the first-time loading, the decreases of compressive strength from the first-time loading to the second-time loading are less than 15 MPa. Meanwhile, the second-time compressive strengths of fiber-reinforced groups are higher than the compressive strength of group F0. These results indicate the significant value and potential of fiber-reinforced AAS composite for its application in engineering. At the age of 60 d, the decreases of compressive strength from the first-time loading to the second-time loading are less than 18 MPa, except for group FPE with a decrease of 32.5 MPa. Most of the samples (except FPE) could retain more than 85% of the compressive strength after the first-time loading at the age of 60 d. Differing from the 3 d samples, the samples start to distort after two times of loading at the age of 60 d, as shown in Fig. 7. It is an interesting and thought-provoking result and will be discussed in the next part.

Since fiber-reinforced samples of group FPE, FAS, FAE, and FSE at 3 d still maintain good shapes after two times of compression loadings (Fig. 7(a)), these tested samples were cured in the fog room again until 60 d for a third-time compression loading, and the results are shown in Fig. 8.

For comparison, the results of samples at other ages were drawn at the same time. The third loading compressive strength of each group is higher than that of the second loading at the age of 3 d. The increased values for group FPE, FAS, FAE and FSE are 11.0 MPa, 13.2 MPa, 14.3 MPa and 13.5 MPa, respectively. Although the third loading compressive strengths are lower than the second loading's at the age of 60 d, they are very close to the compressive strengths at the age of 3 d. Thus it could be deduced that the fiber-reinforced AAS composites have self-healing ability, which possibly owns to the continued reaction of the matrix that supplies reaction products to fill the micro-cracks in samples.

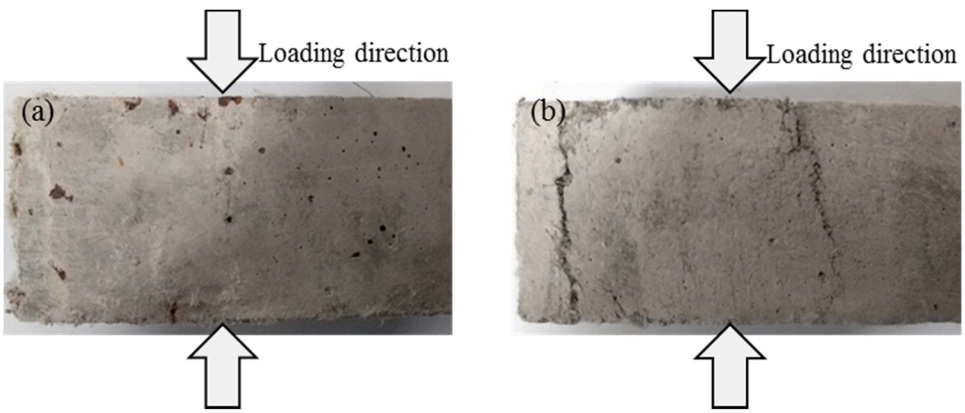

Fig. 7. The sample appearances after two times of loading at the age of: (a) 3 d; (b) 60 d.

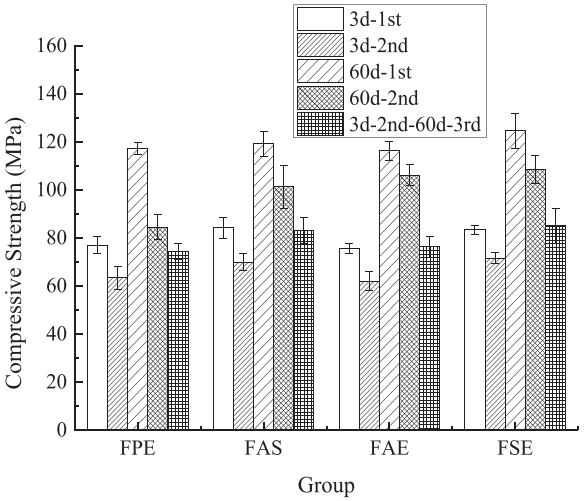

Fig. 8. Comparison of the compressive strength of fiber-reinforced AAS composites with different loading times.

3.3. Uniaxial tensile performance

Fig. 9 shows the uniaxial tensile stress-strain curves of AAS composites prepared with different fibers at the age of 60 d. Each curve represents the testing result of one sample. The stress-strain curves show the strain-hardening property of each sample with single- or hybrid-fibers incorporation. The results show large variations, which is possibly due to the occurrence of eccentric tension during the tests. This implies the fundamental property of the materials and is difficult to avoid. For analysis, the blue curve of each group is picked to be discussed. And the corresponding mechanical parameters of uniaxial tension are shown in Table 4.

It can be seen that group FAE has the highest first cracking tensile strength (σ_{tfc}), followed by group FPVA, with values of 5.8 MPa and 5.2 MPa, respectively. Group FSE has the lowest σ_{tfc}, with a value of 1.3 MPa. Hardening ratio, which is equal to the percentage of $(\sigma_{tu}-\sigma_{tfc})/\sigma_{tfc}$, where σ_{tu} represents ultimate tensile strength, can be a parameter to show hardening capacity. Group FS has the highest hardening ratio. It is because steel fibers have high strength and easy to be dispersed in the matrix. When the matrix cracks, steel fibers bear the extra stress, and the strain-hardening capacity of steel fibers strengthens the sample. It is also the reason for the single-peak-shape curves of group FS. Differing from the multiple micro-cracking of ECC, group FS only has one crack. It means stress is not transmitted but suffered by the steel fibers bridging in the crack during deformation. By contrast, groups with flexible fibers are found with multiple micro-cracking phenomena.

The ultimate tensile strains (ε_{tu}) of single-fibers incorporated groups are higher than 0.7%. PVA fibers are commonly employed to prepare ECC for great performance, and in this paper, the group of FPVA also comes out with the biggest ε_{tu}, with a value of 0.848%. Group FPE has a lower ε_{tu}, with a value of 0.820%. However, the increased value during the strain-hardening stage (ε_{tu}-ε_{tfc}) of group FPE, where ε_{tfc} means first cracking tensile strain, is greater than that of group FPVA, with values of 0.812% and 0.789%, respectively. The lower ε_{tu} but higher ε_{tu}-ε_{tfc} as well as hardening ratio of group FPE compared with group FPVA indicate that for the AAS system, PE fibers may have better reinforce ability for uniaxial tension performance, but the dispersion is still a problem to be solved. Group FS has the lowest ε_{tu} and ε_{tu}-ε_{tfc}. For hybrid-fibers groups, the strain capacities are lower than single-fiber incorporated groups, with values between 0.3% and 0.4%. Because of adding two different kinds of fibers, the amounts of each kind of fiber in samples are lower than that of the single-fibers incorporations. Consequently, the cooperation effect of the same fibers decreases and the reinforced effect decreases accordingly.

The PSH energies (J_b'/J_{tip}, Fig. 10 [38]) of all groups can meet the requirement which is higher than 3 [39]. The PSH energies of group FS and FPE reach 95.9 and 161.0, respectively. However, only two groups (FS and FSE) can meet the requirement of PSH strength (σ_{tu}/σ_{tfc}) which is greater than 1.35 [39].

The absorbed energy can be calculated by integrating the strain-stress curves. Group FAE has the maximum energy absorption capacity, with a value of 66 kJ/m^3, followed by group FPVA, with a value of 48 kJ/m^3.

3.4. Bond behavior between fibers and the matrix

The SEM results of groups FPVA, FPE and FS at the age of 100 d, as well as the PVA and PE fibers are shown in Fig. 11. Images of group FPVA and FPE are magnified 500 and 1000 times. Images of group FS are magnified 100 and 500 times as the steel fiber has a larger diameter than the other two.

The surface of PVA fiber is firmly surrounded by a large amount of reaction products. In contrast, the surfaces of PE fiber and steel fiber have fewer reaction products. It indicates that the reinforcement effects of PVA fibers on the AAS matrix include both friction bonding and chemical bonding, whereas PE and steel fibers only have friction bonding to the AAS matrix. This could be the reason for the highest first cracking and ultimate tensile strengths of group FPVA among the single-fiber-incorporated groups, as shown in Fig. 9

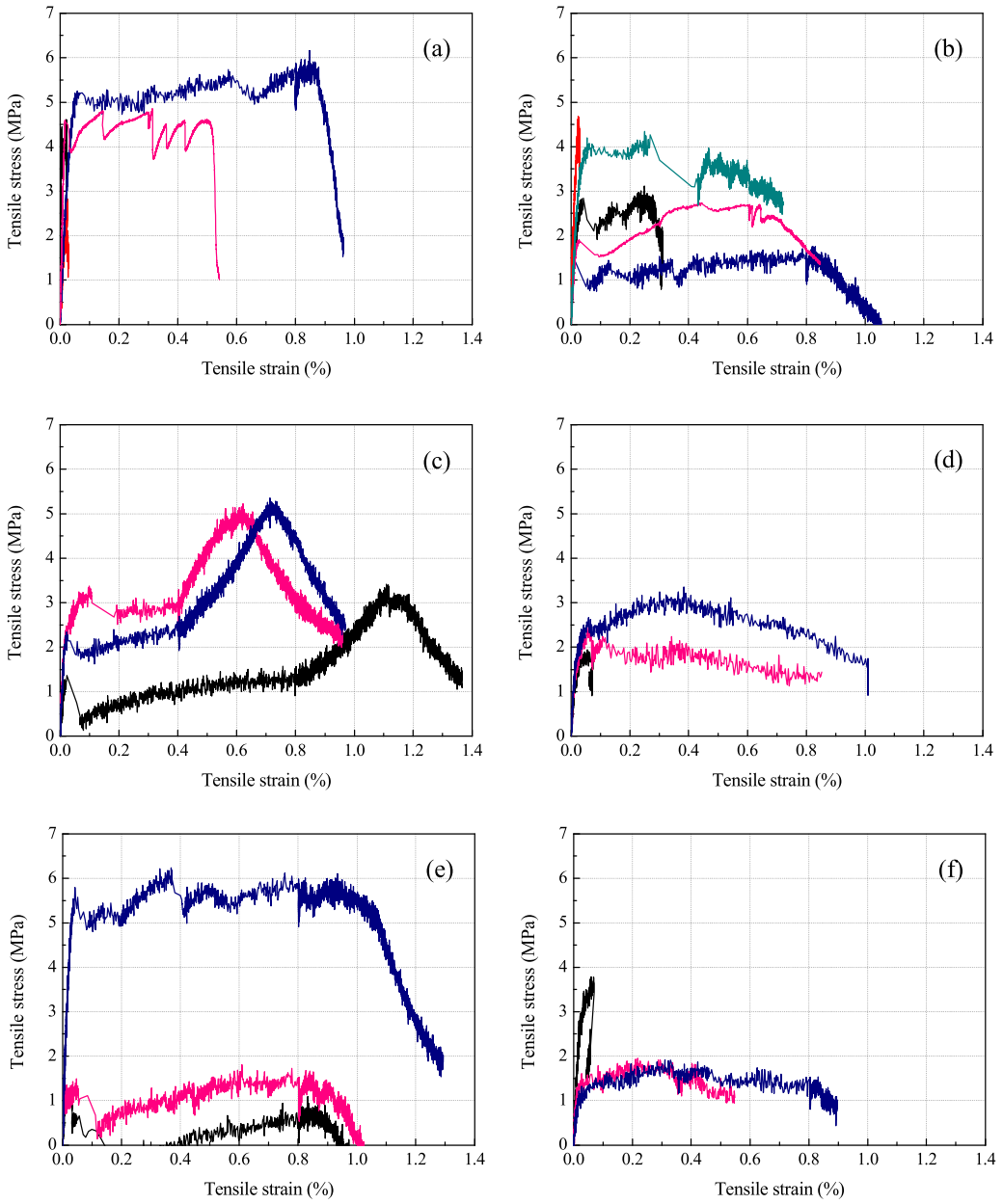

Fig. 9. Uniaxial tensile stress-strain curves of AAS composites prepared with different fibers: (a) FPVA; (b) FPE; (c) FS; (d) FAS; (e) FAE; (f) FSE.

and Table 4.

However, concerning the fibers themselves, it is evident that the morphologies of PVA and PE fibers have been changed. Compared with the original smooth surfaces shown in Fig. 11(g) and (h), PVA fibers in composite are peeled and PE fibers in composite are chapped as shown in Fig. 11(b) and (d), respectively. Differing from the two kinds of polymer fibers, steel fiber has a relatively smooth surface (Fig. 11(f)). It means the PVA and PE fibers will be corroded by waterglass-activated slag matrix with a much higher alkalinity than cement-based materials, while steel fibers have good adaptability in AAS system with a high alkalinity.

4. Discussion

4.1. Reinforcement effect of fibers on the matrix

As mentioned in 3.2, the samples have different appearances after two times of loading between the ages of 3 d and 60 d (Fig. 7). The fiber-reinforced samples do not noticeably change before and after loading at the age of 3 d, while begin to distort at the age of 60

Table 4
Uniaxial tension mechanical parameters of AAS composites prepared with different fibers.

Group	FPVA	FPE	FS	FAS	FAE	FSE
Elasticity Modulus (GPa)	11.54	20.99	12.46	5.92	17.09	5.38
σ_{tfc} (MPa)	5.2	1.4	2.3	2.7	5.8	1.3
ε_{tfc} (%)	0.059	0.008	0.025	0.059	0.042	0.029
σ_{tu} (MPa)	6.2	1.8	5.4	3.4	6.2	1.9
ε_{tu} (%)	0.848	0.820	0.713	0.384	0.369	0.310
σ_{tu}-σ_{tfc} (MPa)	1.0	0.4	3.1	0.7	0.4	0.6
Hardening Ratio (%)	19.2	28.6	134.8	25.9	6.9	46.2
ε_{tu}-ε_{tfc} (%)	0.789	0.812	0.688	0.325	0.327	0.281
PSH strength	1.18	1.30	2.35	1.26	1.08	1.45
PSH energy	8.0	161.0	95.9	5.8	4.2	10.7
Strain-hardening Cracks (n)	6	5	1	7	5	3
Strain-softening Cracks (n)	0	0	0	1	5	3
Average Crack Width (μm)	250	25	3000	75	50	75
Calculated Cracks (n)	6	62	1	8	12	7
Energy Absorption Capacity (kJ/m^3)	48	12	29	25	66	13

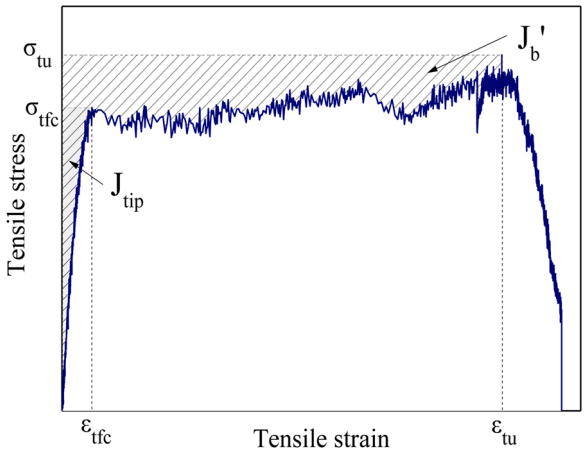

Fig. 10. J_b' and J_{tip} on strain-stress curve for tensile strain-hardening composite (according to [38]).

d. This phenomenon is probably because of the change of brittleness of samples over time. By calculating the flexure to compression ratios of each group (shown in Fig. 12), it can be seen that in general, samples become brittler from 3 d to 60 d. At the same age, the toughening effects of flexible fibers on the matrix are better than that of steel fibers, and the toughening effects of hybrid-fibers groups are between that of each kind of single-fibers group.

The compressive strengths of samples increase about 17.3–38.1 MPa at the age of 60 d by incorporating fibers. These values are similar to those at 3 d which are about 18.3–27.9 MPa (Fig. 6). It could be deduced that at the long age (60 d), the compression reinforcement efficiencies of fibers to the matrix are weaker than those at the early age (3 d). In addition, the reinforcement of fibers to the matrix seems to be time-independent. In other words, there could be an ultimate reinforced strength for fiber-reinforced composites.

As the age grows, the subsequent reaction products are generated, thus the microstructure of matrix is refined and becomes more compacted, as a consequence, the strength keeps developing. One of the reinforced mechanism of fibers to the matrix is bridging. The bridging effect, when the age exceeds a certain value, could be regarded as a static effect on the AAS system which has a fast setting and hardening speed. In other words, the interface bonding between fibers and the matrix probably does not enhance with time and also probably does not enhance with the strengthening of the matrix. It is notable that compared with group F0, the reinforcement efficiency of group FS for compressive strength at the age of 3 d and 60 d are 38.5% and 38.4%, respectively. The results show that there is no reduction in the reinforcement efficiency of steel fibers. This is because besides bridging, lapping, as the other reinforced mechanism of steel fibers to the matrix, can enhance with the strength development of the matrix.

Tables 5 and 6 compare the strength reinforcement efficiencies of fibers in AAS, cement, and geopolymer-based composites at different ages with the data in this paper and literatures [40–45]. Among all data listed in Table 5, the compressive strength reinforcement efficiencies in this paper are the highest, which are over 17% and indicates that all fibers coordinate well with the matrix for the compressive strengths. Meanwhile, the values of compressive strengths of all groups are over 110 MPa at 60 d. These are relatively higher strengths compared with other fiber-reinforced AAMs with strain-hardening property [34–36]. Table 5 shows that the reinforcement efficiencies of fibers to the matrix for compressive strength decrease with the increase of age, except fly ash-based material.

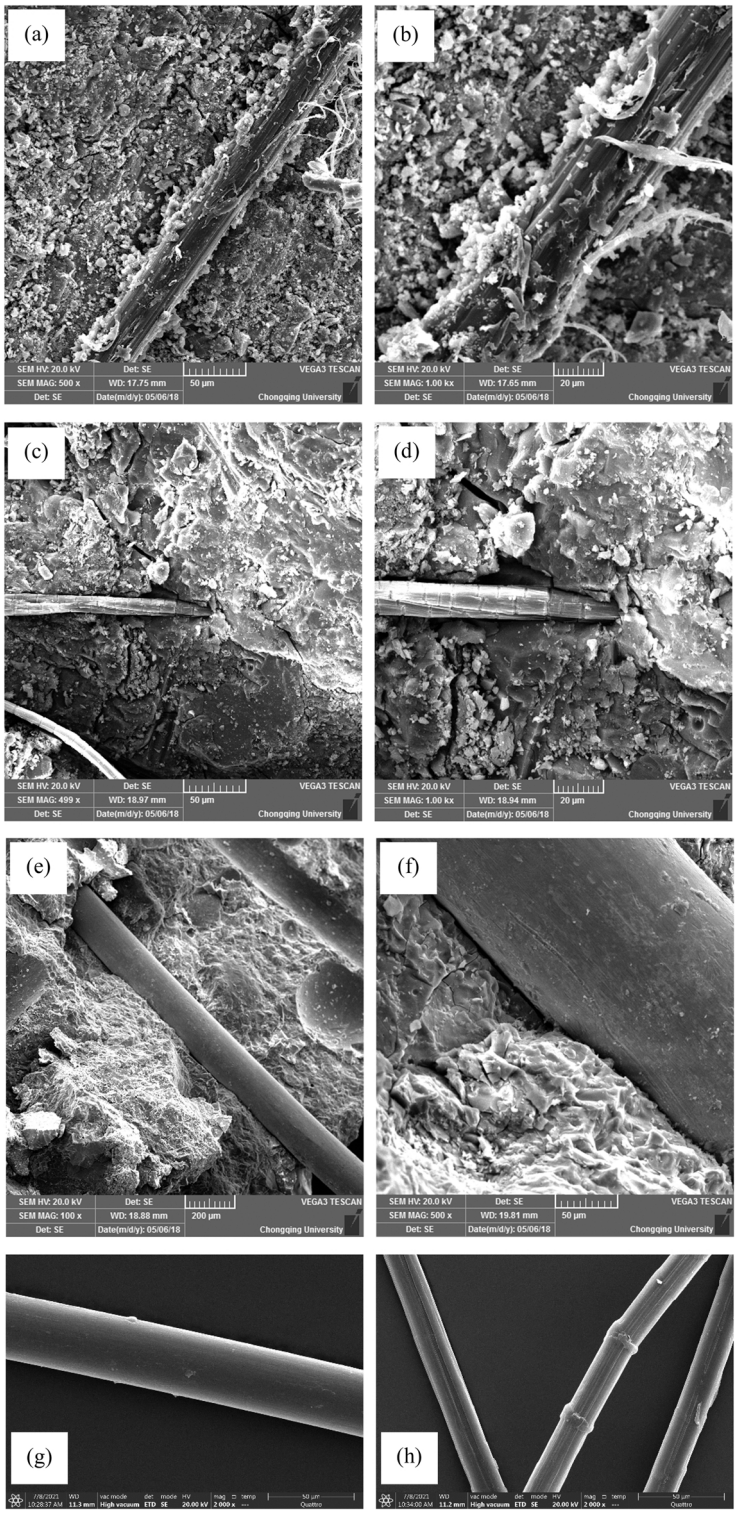

Fig. 11. SEM images of AAS composites with different fibers at 100 d and the original fibers: (a) FPVA 500 × ; (b) FPVA 1000 × ; (c) FPE 500 × ; (d) FPE 1000 × ; (e) FS 100 × ; (f) FS 500 × ; (g) PVA fibers 2000 × ;(h) PE fibers 2000 × .

This exception is mainly because of the decrease of strength of the samples prepared with fly ash-based material. Table 6 shows that the reinforcement efficiencies of fibers to the matrix on flexural strength decrease with age, which is similar with the change on compressive strength. In general, within the scope of data collected in this paper, the reinforcements of fibers, especially of flexible

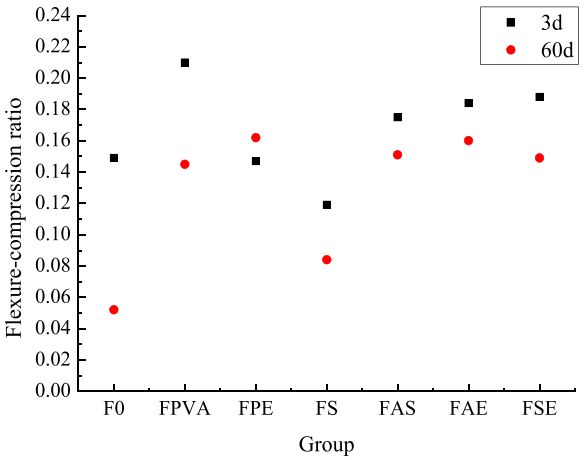

Fig. 12. The flexure to compression ratio of AAS material incorporated with different fibers at the age of 3 d and 60 d.

Table 5
The compressive strength reinforcement efficiencies of fibers in AAS, cement, and geopolymer-based composites at different ages.

Age (d)	Reinforcement efficiency (%)												
	This paper						Yang [40]	Abbass [41]			Varona [42]	Yehia [43]	Al-mashhadani [44]
3	32.5	36.8	38.5	49.6	31.4	48.1	28.0	–	–	–	–	22.5	–
7	–	–	–	–	–	–	–	7.5	11.5	21.2	–	–	3.2
28	–	–	–	–	–	–	10.0	2.7	5.6	8.4	9.9	8.3	4.3
60	17.5	18.1	38.4	20.2	17.4	25.6	–	–	–	–	9.7	–	–

Table 6
The flexural strength reinforcement efficiencies of fibers in AAS, cement, and geopolymer-based composites at different ages.

Age (d)	Reinforcement efficiency (%)			
	Yang [40]	Tian [45]	Yehia [43]	Al-mashhadani [44]
3	207.0	125.0	61.4	–
7	–	–	–	48.9
28	67.0	96.9	22.9	39.8

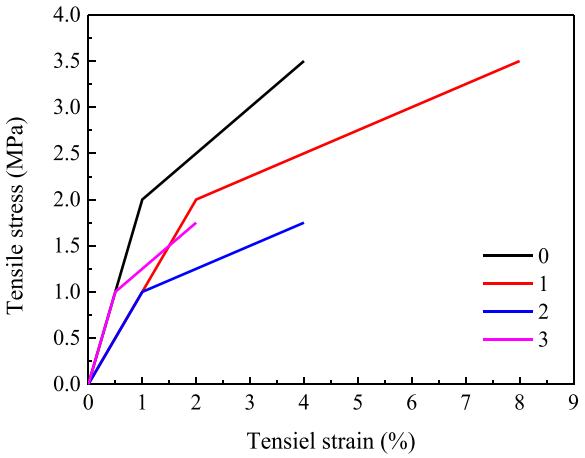

Fig. 13. Schematic of simplified tensile strain-stress curves.

fibers, in different matrixes are static effects, and the reinforcement efficiencies decrease with age.

Except for the static effects mentioned above, the PVA and PE fibers are found to have poor adaptability in waterglass-activated slag system as they can be corroded by the high alkaline environment of the matrix (shown in Fig. 11) which may influence the long-term properties of composites. Corrosion may be another reason for the decrease of compression reinforcement efficiencies of PVA and PE fibers to the matrix with age. At the same time, corrosion may also be the reason for the disappearance of the synergistic effect of the hybrid of flexible fibers and steel fibers at 60 d, as mentioned in 3.2. Therefore, the incorporation of PVA and PE fibers, as well as other polymer fibers in waterglass-activated slag material or AAMs should be cautiously thought and proved.

4.2. Strain-hardening characteristic

As mentioned in 3.3, PSH strength and PSH energy are two important indexes for strain-hardening materials. It is noticeable, however, that comparing these two indexes is not sufficient, particularly when different materials are used. In this paper, even though the strain-stress curve of each group is diverse, there is no obvious difference among the values of PSH strength and PSH energy except for group FPE and FS. To further explain it, the strain-stress curve is simplified into two lines which represent the stage before cracking and the stage during strain-hardening, and the schematic of simplified tensile strain-stress curves is shown in Fig. 13. Note that the strain-softening stage has no effect on PSH strength or PSH energy, thus it is excluded in this part.

After simplification, PSH strength and PSH energy can be written as:

$$\text{PSH strength} = \sigma_{tu}/\sigma_{tfc} \tag{1}$$

$$\text{PSH energy} = \left[1/2 \times \varepsilon_{tfc} \times \sigma_{tfc} + 1/2 \times \left(\varepsilon_{tfc} + \varepsilon_{tu}\right) \times \left(\sigma_{tu} - \sigma_{tfc}\right)\right]/\left(1/2 \times \varepsilon_{tfc} \times \sigma_{tfc}\right) = 1 + \left(\varepsilon_{tfc} + \varepsilon_{tu}\right) \times \left(\sigma_{tu} - \sigma_{tfc}\right)/\varepsilon_{tfc} \times \sigma_{tfc} \tag{2}$$

Suppose

$$\text{PSH strength} = \sigma_{tu}/\sigma_{tfc} = b \tag{3}$$

where $b > 1$, Eq. (2) can be written as:

$$\text{PSH energy} = 1 + \left(\varepsilon_{tfc} + \varepsilon_{tu}\right) \times (b-1)/\varepsilon_{tfc} = 1 + \left(1 + \varepsilon_{tu}/\varepsilon_{tfc}\right) \times (b-1) \tag{4}$$

Suppose

$$\varepsilon_{tu}/\varepsilon_{tfc} = a \tag{5}$$

where $a > 1$, it can be deduced that if two strain-stress curves have the same a and b, they will have the same PSH strength and PSH energy. (It is tenable only under the simplification circumstance. For the real strain-stress curve, the areas are not trapezoid or triangle.).

The four curves in Fig. 13 have the same PSH strength and PSH energy, however, they have discrepant shapes. (Compared with curve 0, curve 1 has the same σ_{tfc} and σ_{tu} but different ε_{tfc} and ε_{tu}; curve 2 has the same ε_{tfc} and ε_{tu} but different σ_{tfc} and σ_{tu}; curve 3 has different σ_{tfc}, σ_{tu}, ε_{tfc} and ε_{tu}.) It is because PSH strength and PSH energy are two relative values. Therefore, to compare the strain-hardening characteristics of different materials, two kinds of absolute values are also needed, for example, elasticity modulus and first cracking strength (σ_{tfc}).

4.3. Number of cracks

The number and the average width of cracks after uniaxial tensile loading are two of the important indexes for strain-hardening fiber-reinforced composites. The crack widths can be measured by using an optical microscope as shown in Fig. 14 and are listed in Table 4. The number of cracks can be calculated according to Eq. (6),

$$N = \left(\varepsilon_{tu} - \varepsilon_{tfc}\right) \times l_0/d \tag{6}$$

where l_0 represents the length of the tested area and d refers to the average crack width.

Nevertheless, this method is relatively rough because of the lower accuracy of the average crack width. In addition, the number of calculated cracks includes the cracks occurring during the stages of strain-hardening and strain-softening. However, it is notable that not all cracks contribute to the strain-hardening behavior. Thus it is important to distinguish the crack numbers during the strain-hardening stage with the ones during the strain-softening stage. This could be achieved by focusing on the tensile stress-strain curves.

Taking group FPVA as an example shown in Fig. 15(a), the uniaxial tensile stress-strain curve is divided into 3 stages, namely before cracking, during strain-hardening, and during strain-softening. When the matrix cracks, fibers begin to bear the load and at the same time, transmit the stress. As a consequence, strain-hardening behavior can be achieved. The manifestation of stress transferring is multiple micro-cracks. In the strain-hardening stage, the slip between fibers and the matrix as well as the elongation of fibers causes the increase of strain. With the increase of strain, the stress increases in fluctuation. Cracks decrease the stress, while fibers increase or maintain the stress. Therefore, the distinct troughs in the stress-strain curve are marked and regarded as the generation of cracks. This cracks-defined method herein proposed is named the trough crack definition.

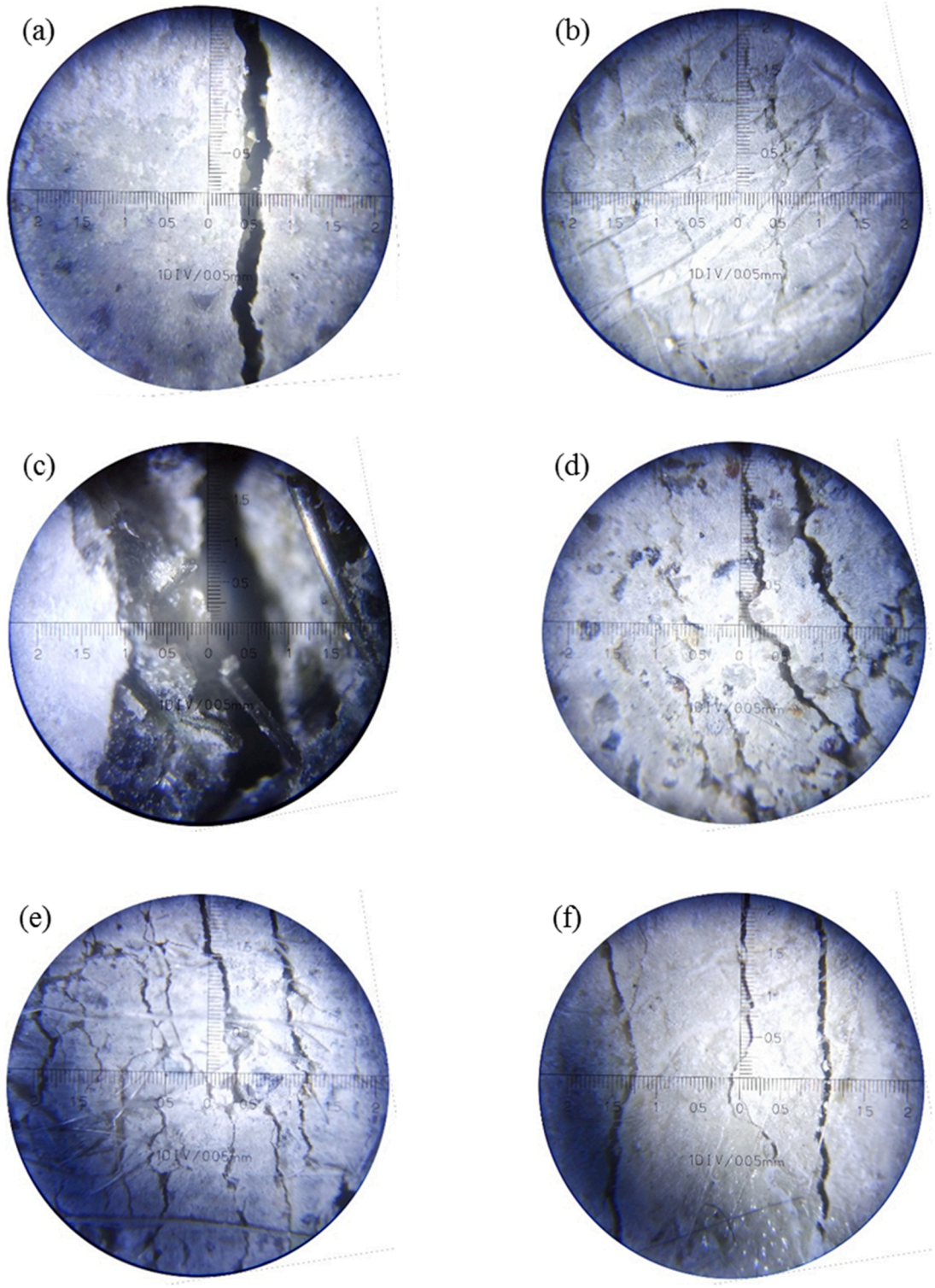

Fig. 14. Cracks after uniaxial tensile loading of AAS composites prepared with different fibers: (a) FPVA; (b) FPE; (c) FS; (d) FAS; (e) FAE; (f) FSE.

According to the trough crack definition, the crack number of each group is shown in Fig. 15(b). For group FS, there is only one trough in the curve, which means that there is only one crack in the sample. The curvature of the curve changes apparently when the strain is around 0.4% (Fig. 9), which means the steel fibers are elongated. The high strain of group FS benefits from the high tensile strength and high toughness of steel fibers. For group FPVA and FPE, although the hardening ratios are not as high as that of group FS,

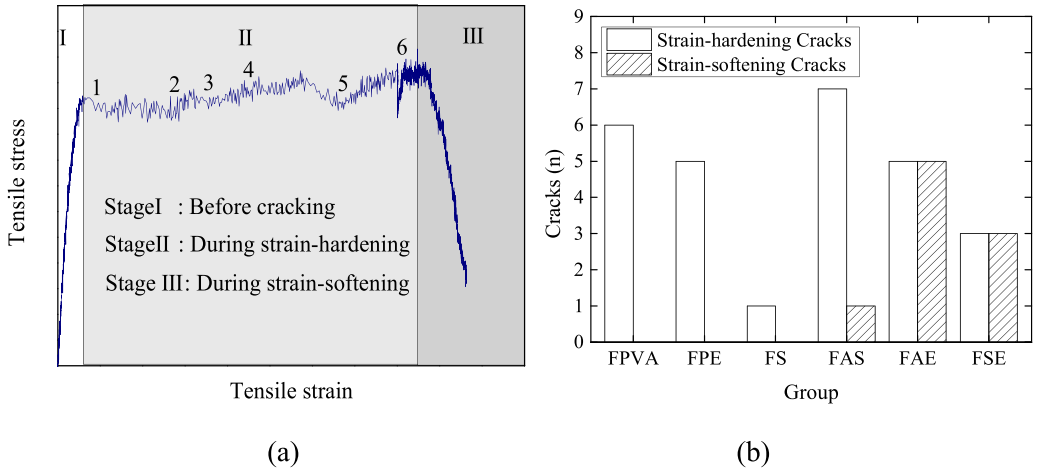

Fig. 15. The trough crack definition: (a) The 3 stages of the uniaxial tensile stress-strain curve for group FPVA and cracks; (b) Crack numbers of different groups.

the stress can keep up or even increase in a long range of strain with the occurrences of multiple micro-cracks in the samples. The increases of strain during the strain-hardening stage are smaller for groups with hybrid fibers compared with groups with single fibers. In the strain-hardening stage, the samples of group FAS and FAE show 5–7 cracks, while the sample of group FSE only has 3 cracks. Therefore, it can be deduced that for multiple-cracking mechanism induced strain-hardening property, the reinforced effect of PVA fibers is better than that of PE fibers, and the effect of steel fibers is inferior in the system of this study.

The stage of strain-softening reflects the bearing capacity when the ultimate tensile strain is exceeded. In this stage, it can be found (Fig. 9) that the stress of group FPVA decreases rapidly, followed by group FS and FPE. However, the three groups with hybrid fibers show slowly decline on tensile stress. It indicates that the samples of these groups can still keep the capacities of load-bearing and deformation to a certain degree when the loads exceed their ultimate tensile stresses. It is interesting that different from the group with single fibers, groups with hybrid fibers still have troughs in their curves. In other words, there are new micro-cracks occurring during this stage. This phenomenon benefits from the time lag of the reinforced effect of different fibers, which is induced by different stress states. Fibers have different properties, including elastic modulus, tensile strength, ductility, as well as bonding and friction with the matrix. Therefore, each kind of fiber has different slips with the matrix, different elongation and stress states. As a consequence, hybrid incorporations make the reinforcement effect of fibers reduced and evenly distributed under uniaxial tensile loading.

Fig. 16 shows the comparison of defined and calculated cracks numbers. The defined cracks are obtained by using the trough crack definition proposed in this paper. Note that the defined cracks here include cracks occurring in the stage of strain-hardening and strain-softening. The red line is the fitting result of points except for the red dot, with a slope of 1.17 and r^2 of 0.96. The blue line has a slope of 1. These two methods match well, hence the trough crack definition provides a possible way to number cracks and thus to characterize the strain-hardening property of fiber-reinforced composites.

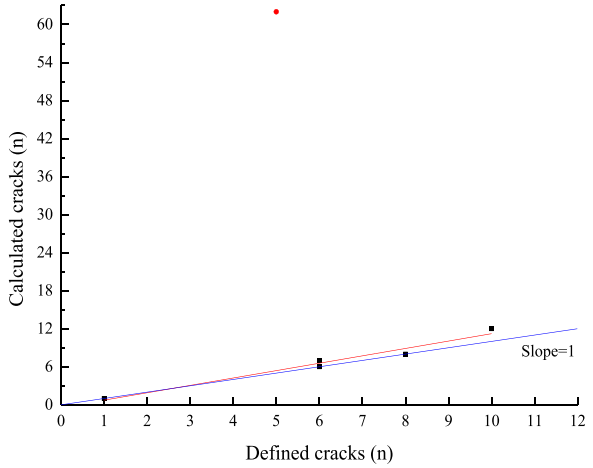

Fig. 16. The comparison of defined and calculated cracks numbers.

5. Conclusion

This paper uses PVA, PE, and steel fibers, as well as the hybrids of two of these three fibers to obtain high strength strain-hardening AAS composites. The reinforcement effects of fibers on AAS material are as follows.

Flexible fibers (i.e. PVA and PE fibers) contribute more to the flexural strength of AAS composites compared with steel fibers, while steel fibers are more effective for the reinforcement of the compressive strength of AAS material. However, deteriorations of PVA and PE fibers are found in AAS material with a high alkalinity, which may influence the long-term properties of composites. The hybrids of flexible fibers and steel fibers have a synergistic effect on the compressive strength at 3 d. The incorporation of fibers not only increases the compressive and flexural strength of samples but also changes their failure mode. The fiber-reinforced AAS composites retain more than 80% of their strength after the first-time test. And the composites have the potential of self-healing ability at an early age. The reinforcement of flexible fibers to the matrix is a static effect, and the reinforcement efficiency decreases with age.

Strain-hardening behavior is achieved by the incorporation of PVA, PE and steel fibers. The mechanism causing tensile strain-hardening behavior of PVA and PE fiber-reinforced AAS composites is multiple cracking, while that of steel fiber-reinforced AAS composite is single cracking. The composite reinforced by PVA fibers shows the biggest tensile strain in this paper. PE fiber-reinforced AAS composite has the highest strain capacity during the strain-hardening stage, but the dispersion of PE fibers in the matrix is still a problem to be solved. Hybrid incorporations make the reinforcement effect of fibers reduced and evenly distributed under uniaxial tension, with samples showing the slowly decline of stress during the strain-softening stage.

For characterizing the strain-hardening property, a method to define the number of cracks in samples is proposed, which is based on the number of troughs in uniaxial tensile stress-strain curves. This method is more reasonable because it can distinguish the cracks occurring during the strain-hardening stage or strain-softening stage.

CRediT authorship contribution statement

Yaowen Xu: Conceptualization, Methodology, Formal analysis, Investigation, Writing – original draft. **Chaojun Wan:** Conceptualization, Writing – review & editing, Supervision, Project administration, Funding acquisition. **Xuhui Liang:** Formal analysis, Investigation, Writing – review & editing. **Hongyu Yang:** Writing – review & editing, Supervision.

Declaration of Competing Interest

The authors declare that they have no known competing financial interests or personal relationships that could have appeared to influence the work reported in this paper.

Data Availability

Data will be made available on request.

Acknowledgments

All authors would like to acknowledge the financial support of the Chongqing Science and Technology Commission of China under Grant No. cstc2014gjhz50001 named International Joint Research and Development Centre of Low Carbon and High Performance Cement-Based Materials.

References

[1] P. Tomar, R. Lakhani, V.K. Chhibber, R. Kumar, Macro-defect free cements: a future oriented polymer composite materials for construction industries, Compos. Interfaces 25 (2018) 607–627, https://doi.org/10.1080/09276440.2018.1439637.
[2] P. Kinnunen, A. Ismailov, S. Solismaa, H. Sreenivasan, M.-L. R€ais€anen, E. Lev€anen, M. Illikainen, Recycling mine tailings in chemically bonded ceramics - A review, J. Clean. Prod. J. 174 (2018) 634–649, https://doi.org/10.1080/09276440.2018.1439637.
[3] H.A. Goaiz, T. Yu, M.N.S. Hadi, Quality evaluation tests for tensile strength of reactive powder concrete, J. Mater. Civ. Eng. 30 (2018), 04018070, https://doi.org/10.1061/(asce)mt.1943-5533.0002257.
[4] Y. Farnam, M. Moosavi, M. Shekarchi, S.K. Babanajad, A. Bagherzadeh, Behaviour of slurry infiltrated fibre concrete (SIFCON) under triaxial compression, Cem. Concr. Res. 40 (2010) 1571–1581, https://doi.org/10.1016/j.cemconres.2010.06.009.
[5] J.Y. Wang, J.Y. Guo, Damage investigation of ultra high performance concrete under direct tensile test using acoustic emission techniques, Cem. Concr. Compos. 88 (2018) 17–28, https://doi.org/10.1016/j.cemconcomp.2018.01.007.
[6] K. Yu, L. Li, J. Yu, Y. Wang, J. Ye, Q.F. Xu, Direct tensile properties of engineered cementitious composites: a review, Constr. Build. Mater. 165 (2018) 346–362, https://doi.org/10.1016/j.conbuildmat.2017.12.124.
[7] V.C. Li, C.K.Y. Leung, Steady-state and multiple cracking of short random fiber composites, J. Eng. Mech. 118 (1992) 2246–2264.
[8] Y. Yang, E.H. Yang, V.C. Li, Autogenous healing of engineered cementitious composites at early age, Cem. Concr. Res. 41 (2011) 176–183, https://doi.org/10.1016/j.cemconres.2010.11.002.
[9] S. Qian and V.C. Li, Headed Anchor / Engineered Cementitious Composites (ECC) Pullout Behavior, 9 (2011) 339–351.
[10] M. Ohno, V.C. Li, A feasibility study of strain hardening fiber reinforced fly ash-based geopolymer composites, Constr. Build. Mater. 57 (2014) 163–168, https://doi.org/10.1016/j.conbuildmat.2014.02.005.
[11] X. Huang, R. Ranade, W. Ni, V.C. Li, Development of green engineered cementitious composites using iron ore tailings as aggregates, Constr. Build. Mater. 44 (2013) 757–764, https://doi.org/10.1016/j.conbuildmat.2013.03.088.
[12] D. Desai, M. Miller, J.P. Lynch, V.C. Li, Development of thermally adaptive engineered cementitious composite for passive heat storage, Constr. Build. Mater. 67 (2014) 366–372, https://doi.org/10.1016/j.conbuildmat.2013.12.104.

[13] R. Ranade, J. Zhang, J.P. Lynch, V.C. Li, Influence of micro-cracking on the composite resistivity of engineered cementitious composites, Cem. Concr. Res. 58 (2014) 1–12, https://doi.org/10.1016/j.cemconres.2014.01.002.
[14] V.W.J. Lin, M. Li, J.P. Lynch, V.C. Li, Mechanical and electrical characterization of self-sensing carbon black ECC, Proc. SPIE Int. Soc. Optic. Eng. (2011), 798316, https://doi.org/10.1117/12.880178.
[15] M. Li, V.C. Li, Rheology, fiber dispersion, and robust properties of engineered cementitious composites, Mater. Struct. Constr. 46 (2013) 405–420, https://doi.org/10.1617/s11527-012-9909-z.
[16] K. Yu, Y. Wang, J. Yu, S. Xu, A strain-hardening cementitious composites with the tensile capacity up to 8%, Constr. Build. Mater. 137 (2017) 410–419, https://doi.org/10.1016/j.conbuildmat.2017.01.060.
[17] P. Stynoski, P. Mondal, C. Marsh, Effects of silica additives on fracture properties of carbon nanotube and carbon fiber reinforced Portland cement mortar, Cem. Concr. Compos. 55 (2015) 232–240, https://doi.org/10.1016/j.cemconcomp.2014.08.005.
[18] S. Yeşilmen, Y. Al-Najjar, M.H. Balav, M. Şahmaran, G. Yildirim, M. Lachemi, Nano-modification to improve the ductility of cementitious composites, Cem. Concr. Res. 76 (2015) 170–179, https://doi.org/10.1016/j.cemconres.2015.05.026.
[19] H.J. Kong, S.G. Bike, V.C. Li, Development of a self-consolidating engineered cementitious composite employing electrosteric dispersion/stabilization, Cem. Concr. Compos. 25 (2003) 301–309, https://doi.org/10.1016/S0958-9465(02)00057-4.
[20] H. Stang, V.C. Li, Extrusion of ECC-material, high perform, Fiber Reinf. Cem. Compos. 3 (HPFRCC 3) (1999) 203–212.
[21] Y.Y. Kim, H.J. Kong, V.C. Li, Design of engineered cementitious composite suitable for wet-mixture shotcreting, Acids Mater. J. 100 (2003) 511–518, https://doi.org/10.14359/12958.
[22] V.C. Li, On engineered cementitious composites (ECC), J. Adv. Concr. Technol. 1 (2003) 215–230, https://doi.org/10.3151/jact.1.215.
[23] B. Zhu, J. Pan, B. Nematollahi, Z. Zhou, Y. Zhang, J. Sanjayan, Development of 3D printable engineered cementitious composites with ultra-high tensile ductility for digital construction, Mater. Des. 181 (2019), 108088, https://doi.org/10.1016/j.matdes.2019.108088.
[24] S. Muzenski, I. Flores-Vivian, K. Sobolev, Hydrophobic engineered cementitious composites for highway applications, Cem. Concr. Compos. 57 (2015) 68–74, https://doi.org/10.1016/j.cemconcomp.2014.12.009.
[25] T.K. Erdem, Specimen size effect on the residual properties of engineered cementitious composites subjected to high temperatures, Cem. Concr. Compos. 45 (2014) 1–8, https://doi.org/10.1016/j.cemconcomp.2013.09.019.
[26] Q. Zhang, V.C. Li, Development of durable spray-applied fire-resistive engineered cementitious composites (SFR-ECC), Cem. Concr. Compos. 60 (2015) 10–16, https://doi.org/10.1016/j.cemconcomp.2015.03.012.
[27] A. Zhao, J. Yang, E.H. Yang, Self-cleaning engineered cementitious composites, Cem. Concr. Compos. 64 (2015) 74–83, https://doi.org/10.1016/j.cemconcomp.2015.09.007.
[28] M.B. Weimann, V.C. LI, Drying shrinkage and crack width of engineered cementitious composites (Ecc), Inst. Fundam. Technol. Res. (2003), https://doi.org/10.1533/9780857093103.37.
[29] V.C. Li, M. Lepech, S. Wang, Development of green engineered cementitious composites for sustainable infrastructure systems, Int. Work. Sustain. Dev. Concr. Technol. 1 (2004) 181–191. ⟨http://core.kmi.open.ac.uk/download/pdf/11346106.pdf#page=192⟩.
[30] M. Şahmaran, V.C. Li, Durability properties of micro-cracked ECC containing high volumes fly ash, Cem. Concr. Res. 39 (2009) 1033–1043, https://doi.org/10.1016/j.cemconres.2009.07.009.
[31] J. Zhou, S. Qian, M.G.S. Beltran, G. Ye, K. Van Breugel, V.C. Li, Development of engineered cementitious composites with limestone powder and blast furnace slag, Mater. Struct. Constr. 43 (2010) 803–814, https://doi.org/10.1617/s11527-009-9549-0.
[32] A. Fernández-Jiménez, J.G. Palomo, F. Puertas, Alkali-activated slag mortars: mechanical strength behaviour, Cem. Concr. Res 29 (1999) 1313–1321, https://doi.org/10.1016/S0008-8846(99)00154-4.
[33] G. Görhan, G. Kürklü, The influence of the NaOH solution on the properties of the fly ash-based geopolymer mortar cured at different temperatures, Compos. Part B Eng. 58 (2014) 371–377, https://doi.org/10.1016/j.compositesb.2013.10.082.
[34] B.Y. Lee, C.G. Cho, H.J. Lim, J.K. Song, K.H. Yang, V.C. Li, Strain hardening fiber reinforced alkali-activated mortar - a feasibility study, Constr. Build. Mater. 37 (2012) 15–20, https://doi.org/10.1016/j.conbuildmat.2012.06.007.
[35] J. Il Choi, B.Y. Lee, R. Ranade, V.C. Li, Y. Lee, Ultra-high-ductile behavior of a polyethylene fiber-reinforced alkali-activated slag-based composite, Cem. Concr. Compos. 70 (2016) 153–158, https://doi.org/10.1016/j.cemconcomp.2016.04.002.
[36] B. Nematollahi, J. Sanjayan, F.U.Ahmed Shaikh, Tensile strain hardening behavior of PVA FIber-reinforced Engineered Geopolymer Composite, J. Mater. Civ. Eng. 27 (2015), 04015001, https://doi.org/10.1061/(asce)mt.1943-5533.0001242.
[37] Y. Xu, Study on alkali-activated slag composite with engineer ed m atrix in coor dination with several fibers, Chongqing University, 2018.
[38] E. Yangand V.C. Li, A Micromechanical Model for Fiber Cement Optimization and Component Tailoring, 10th Int. Inorganic-Bonded Fiber Compos. Conf. (2006) 1–13.
[39] T. Kanda, V.C. Li, Practical design criteria for saturated pseudo strain hardening behavior in ECC, J. Adv. Concr. Technol. 4 (2006) 59–72, https://doi.org/10.3151/jact.4.59.
[40] Q. Yang, Study on preparation of green engineered cementitious composites u sing alkali-activated slag, Chongqing University, 2016.
[41] W. Abbass, M.I. Khan, S. Mourad, Evaluation of mechanical properties of steel fiber reinforced concrete with different strengths of concrete, Constr. Build. Mater. 168 (2018) 556–569, https://doi.org/10.1016/j.conbuildmat.2018.02.164.
[42] F.B. Varona, F.J. Baeza, D. Bru, S. Ivorra, Influence of high temperature on the mechanical properties of hybrid fibre reinforced normal and high strength concrete, Constr. Build. Mater. 159 (2018) 73–82, https://doi.org/10.1016/j.conbuildmat.2017.10.129.
[43] S. Yehia, A.E. Douba, O. Abdullahi, S. Farrag, Mechanical and durability evaluation of fiber-reinforced self-compacting concrete, Constr. Build. Mater. 121 (2016) 120–133, https://doi.org/10.1016/j.conbuildmat.2016.05.127.
[44] M.M. Al-mashhadani, O. Canpolat, Y. Aygörmez, M. Uysal, S. Erdem, Mechanical and microstructural characterization of fiber reinforced fly ash based geopolymer composites, Constr. Build. Mater. 167 (2018) 505–513, https://doi.org/10.1016/j.conbuildmat.2018.02.061.
[45] S. Tian, Preparation and properties of cement-based materials reinforced with carbon nanotubes and PVA fibers, Chongqing University, 2014.